Spin-wave stiffness of the Dzyaloshinskii-Moriya helimagnet compounds $Fe_{1-x}Co_xSi$ studied by small-angle neutron scattering

S. V. Grigoriev,[1,2,3] K. A. Pschenichnyi,[1,2,3] E. V. Altynbaev,[1,2,3] S.-A. Siegfried,[4] A. Heinemann,[4] D. Honnecker,[5] and D. Menzel[6]

[1]*Petersburg Nuclear Physics Institute NRC "Kurchatov Institute", Gatchina, St-Petersburg 188300, Russia*
[2]*Saint-Petersburg State University, Ulyanovskaya 1, Saint-Petersburg 198504, Russia*
[3]*Institute for High Pressure Physics, Russian Academy of Sciences, 142190 Troitsk, Moscow, Russia*
[4]*Helmholtz Zentrum Geesthacht, Geesthacht 21502, Germany*
[5]*Institute Laue Langevin, Grenoble, 38042 Grenoble, Cedex 9, France*
[6]*Technische Universität Braunschweig, 38106 Braunschweig, Germany*

(Received 5 January 2019; revised manuscript received 29 July 2019; published 5 September 2019)

The spin wave stiffness was measured by small-angle neutron scattering method in the Dzyaloshinskii-Moriya helimagnet compounds $Fe_{1-x}Co_xSi$ with $x = 0.25, 0.30, 0.50$. It has been shown that the spin wave dispersion in the fully polarized state is anisotropic due to Dzyaloshinskii-Moriya interaction. It is reflected in the neutron scattering pattern as two circles for neutrons obtaining and losing the magnon energy, respectively. The centers of the circles are shifted by the momentum transfer oriented along the applied magnetic field **H** and equal to the wave vector of the spiral $\pm\mathbf{k}_s$. The radius of the circles is directly related to the stiffness of spin waves and depends on the magnetic field. We have found that the spin-wave stiffness A change weakly with temperature for each individual compound. On the other hand, the spin-wave stiffness A increases linearly with x in contrast to the x dependences of the critical temperature T_c and the low-temperature ordered moment. Experimentally obtained values of the stiffness A approve quantitative applicability of the Bak-Jensen model for the compounds under study.

DOI: 10.1103/PhysRevB.100.094409

I. INTRODUCTION

In recent years the exotic spin systems, which are formed as a result of a balance between the ferromagnetic exchange interaction and the Dzyaloshinskii-Moriya exchange antisymmetric interaction, have attracted particular interest [1–19]. The Dzyaloshinskii-Moriya interaction (DMI) emerges as a result of a lack of an inversion symmetry in cubic crystals with the $P2_13$ space group. It is the ratio between the ferromagnetic interaction with the constant J and the DMI with the constant D that determines the magnitude of the helix wave vector or skyrmion array $k_s = D/J$ [1,2]. Moreover, the constants D and J determine the energy landscape of the magnetic system and its spin dynamics.

Though most of researchers attention has been drawn to the manganese monosilicide MnSi [3–5], other archetypical compounds $Fe_{1-x}Co_xSi$ have also demonstrated many intriguing properties. First of all, these compounds $Fe_{1-x}Co_xSi$ order below T_c in a homochiral spin helical structure in the range of $x \in [0.05; 0.8]$ [6–9]. The critical temperature T_C shows a slightly asymmetric bell-like shape as a function of the Co concentration x with a maximum at $x \sim 0.40$. Secondly, all of them demonstrate the appearance of the skyrmion lattice in the tiny pocket of the $(H - T)$ phase diagram close to the critical temperature T_c [8–12]. Another intriguing feature observed in the mixed compounds $Fe_{1-x}Co_xSi$ [13] (as well as in $Mn_{1-x}Fe_xGe$ [14,15] and $Fe_{1-x}Co_xGe$ [16]) is a flip of the link between crystallographic and magnetic chiralities upon mixing the two different magnetic atoms Fe and Co (or, Mn and Fe). Theoretical investigations suggest to ascribe the flip of the helix chirality as a function of x to a change of sign of the DMI constant [17–19]. As was shown in Ref. [13] that the spin helix in $Fe_{1-x}Co_xSi$ compounds transforms to a ferromagnet ($|\mathbf{k}| \to 0$) at a critical concentration $x_c \approx 0.65$ at low temperature ($T \approx 3$ K). This transformation is accompanied by the change of the link between structural and magnetic chiralities for $x < x_c$ and $x > x_c$. For FeSi-based compounds ($x < x_c$) the right-/left-handed crystalline chirality is accompanied by the left-/right-handedness of the magnetic helix ($\Gamma_c \times \gamma_m = -1$), while the CoSi-based compounds ($x > x_c$) show the right handed lattice chirality along with the right handedness of the magnetic spiral ($\Gamma_c \times \gamma_m = 1$). Here Γ_c is the crystal chirality, and γ_m is the magnetic chirality taking the value -1 for the right handed or 1 for the left handed chiralities.

Another important experimental parameter characterizing the system is the magnitude of the external magnetic field H_{C2}, which must be applied in order to transform the spin helix into a collinear spin structure (fully polarized state). It is shown that the energy difference $g\mu_B H_{C2}$ between the fully polarized state and the spiral state is Ak_s^2, where $A = SJ$ is the spin-wave stiffness and S is the ordered spin [20,21]. One can estimate the spin wave stiffness using the relation $Ak_s^2 = g\mu_B H_{C2}$. Such an estimate made for the spin wave stiffness ($T = 0$ K) of the compounds $Fe_{1-x}Co_xSi$ shows a linear dependence of A on the concentration in the range of x from 0.1 to 0.6 [10]. The linear x dependence demonstrates no correlation with the critical temperature T_C, which shows a bell-like shape

function on x with a maximum at $x \sim 0.40$ [13]. Similarly, the saturation magnetization measurements show that the ordered moment per metallic atom in $Fe_{1-x}Co_xSi$ compounds has the bell-like x dependence with a maximum at $x \sim 0.40$ [22]. As was noticed above the value of the helix wave vector k shows nonmonotonous (even oscillating) behavior as a function of the concentration x [13]. Therefore it is surprising that theoretical estimates of the spin-wave stiffness A show linear increase with concentration x. The direct measurements of the spin wave stiffness using neutron scattering have not been performed in these compounds and, therefore, it was difficult to confirm or disprove the conclusions of work [10].

In this paper we have used a recently proposed method of small-angle neutron scattering to measure the spin wave stiffness in the Dzyaloshinskii-Moriya helimagnet compounds $Fe_{1-x}Co_xSi$. We have found that the spin-wave stiffness A increases linearly with x. The measured values are in good agreement with the theoretical predictions given on the basis of Bak-Jensen theory [10].

II. EXPERIMENT

As was recently shown the low energy spin waves in the helimagnetics with the DM interaction are strongly anisotropic even in the fully polarized state [23]. The spin-wave energy in this case was explicitly given by Kataoka in Ref. [24]:

$$\epsilon_{\mathbf{q}} = A(\mathbf{q} - \mathbf{k}_s)^2 + (H - H_{C2}), \tag{1}$$

where $\mathbf{k_s}$ matches with the orientation of the external magnetic field. The sign of the DM constant determines the direction of the helix wave vector k_s being parallel or antiparallel with respect to the direction of the field. Here and further on we omit the factor $g\mu_B$ at the value of the field H for simplicity but imply H is measured in the energy units. This form of the spin wave dispersion causes the nonreciprocity of the spin-wave propagation demonstrated in fully polarized helimagnet compounds with DM interaction [25,26].

The validity of the spin-wave dispersion [Eq. (1)] has been experimentally proven for MnSi using the small-angle polarized neutron scattering [23]. It was demonstrated that the sign of the DM constant determines a preferable clockwise or anticlockwise rotation of the spin waves, i.e., the chirality of the DM helimagnet compounds results in one-handed excitations in the full-polarized state. Analysis of the scattering patterns allows one to measure the spin-wave stiffness A as a function of temperature. Conclusions derived in Ref. [23] on the basis of SANS measurements have been proven once again using triple-axis spectroscopy [27]. The complementarity of these two methods has been clearly discussed in Ref. [23].

It was analytically shown that the inelastic neutron scattering in the case of DM helimagnet compounds is concentrated mostly around the momentum transfers corresponding to $\pm\mathbf{k}_s$ within two narrow cones limited by the cutoff angle θ_C for the energy gain/energy loss, respectively [23]. The cutoff angle θ_C is connected to the spin-wave stiffness A via the dimensionless parameter $\theta_0 = \hbar^2/(2Am_n)$:

$$\theta_C^2(H) = \theta_0^2 - \frac{\theta_0}{E_i}H + \theta_B^2, \tag{2}$$

where m_n is the neutron mass, θ_B is the Bragg angle of the scattering on spin spiral with the length $2\pi/k_s$, and E_i denotes the energy of incident neutrons.

Following the protocol of measurements given in Ref. [23], we have determined the spin-wave stiffness in the fully polarized state for the $Fe_{1-x}Co_xSi$ compounds using the small-angle neutron scattering method. High-purity single crystals of the $Fe_{1-x}Co_xSi$ with $x = 0.30$ and 0.50, grown by the Chokhralski method, were chosen for this study. They were disks with diameter of the order of 8 mm and thickness of the order of 1 mm.

The small-angle neutron scattering experiments were performed with $Fe_{0.70}Co_{0.30}Si$ and $Fe_{0.50}Co_{0.50}Si$ compounds at the instrument SANS-1 ($\lambda = 0.5$ nm) at the FRM-II reactor at the MLZ (Germany). The ordering temperature of these compounds is $T_c = 47$ K and $T_c = 42$ K, the critical field of the transition to the fully polarized state is $H_{C2} = 0.17$ T and $H_{C2} = 0.05$ T, and the helix wave vector $k = 0.16$ nm^{-1} and $k = 0.068$ nm^{-1}, respectively. A magnetic field up to 2 T was applied along Q_x perpendicular to the neutron beam. The [110] axis of the single crystals was oriented parallel to the applied field with accuracy of 5°. Background intensity maps were taken for all samples at low temperature ($T = 5$ K) and high magnetic field ($H = 2$ T) when both the elastic magnetic peak and spin wave scattering are fully suppressed. These background maps were subtracted from the other scattering maps of a given sample. We used the data-reduction software GRASP developed at the ILL, Grenoble [28].

The similar SANS experiment had been performed recently for the $Fe_{0.75}Co_{0.25}Si$ compound at the instrument D11 ($\lambda = 0.6$ nm) at the Laue-Langevin Institute (Grenoble, France) [29]. The ordering temperature of this compound is $T_c = 38$ K, and the critical field is $H_{C2} = 0.18$ T and the helix wave vector $k = 0.19$ nm^{-1}. The data obtained for this compound are added to this work for completeness.

III. RESULTS

Figure 1(a) shows a typical map of the small-angle neutron scattering intensity for the compound $Fe_{0.70}Co_{0.30}Si$ at a temperature below T_c and in a magnetic field below H_{C2}. The Bragg reflections at $\mathbf{Q} = \pm\mathbf{k}_s$ are clearly seen in Fig. 1(a) due to scattering by the spiral structure with the wave vector $\pm\mathbf{k}_s$ directed along the applied field $\mathbf{H}$. The wave vector k_s depends weakly on temperature and is equal to 0.16 nm^{-1} at $T = 5$ K and to 0.147 nm^{-1} at $T = 40$ K.

At fields exceeding the critical field H_{C2}, the elastic neutron scattering (Bragg peaks) disappears completely and inelastic scattering remains only, concentrated around $\mathbf{Q} = \pm\mathbf{k}_s$ [Fig. 1(b)]. This scattering intensity is collected within a circular spot limited by the cutoff angle θ_C. For nonpolarized neutron experiments one can detect two Bragg reflections at $\mathbf{Q} = \pm\mathbf{k}_s$ as in Fig. 1(a). It is known that the neutrons after scattering events became polarized: The incident neutrons with the spins parallel to the field are reflected to the right spot but those with the spins opposite the field are scattered to the left spot [30]. For the sake of statistics of the inelastic experiment we conducted measurements with nonpolarized neutrons. As a result two circular spots centered at $\mathbf{Q} = \pm\mathbf{k}_s$ overlap, as seen in Fig. 1(b). Nevertheless, the clear cutoff of

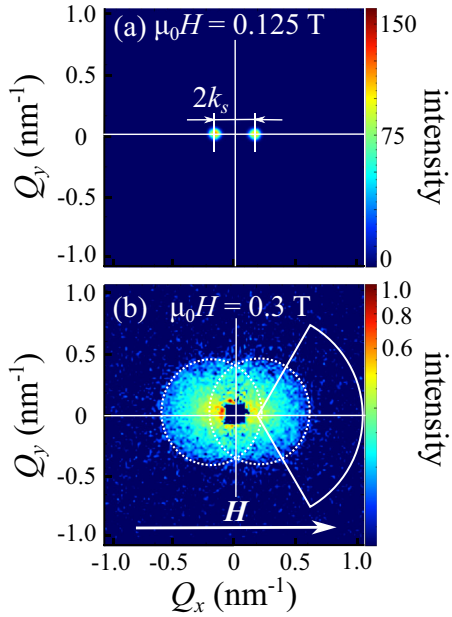

FIG. 1. Maps of the small-angle neutron scattering at $T = 15$ K for $Fe_{0.7}Co_{0.3}Si$: (a) in the conical phase at magnetic field $\mu_0 H = 0.125$ T, (b) in the induced ferromagnetic phase at magnetic field $\mu_0 H = 0.3$ T.

the spots allows one to separate both spots [shown by a dashed circles in Fig. 1(b)].

These circular spots with the center at $\mathbf{Q} = \mathbf{k}_s$ can be observed in a wide range of fields up to $H_{\text{off}} = \theta_0 E_i$ of the order of 1 T for this compound [according to Eq. (2)]. A size of these spots shrinks remarkably with the field as can be seen in Figs. 2(a)–2(c). The cutoff angle of neutron scattering θ_C related to the spin wave stiffness can be easily estimated from these data.

To further improve the statistics, the scattering intensity of the SANS maps was azimuthally-averaged over the angular sector of 120 degrees with the center positioned at $\boldsymbol{Q} = \pm \boldsymbol{k}_s$ as shown in Fig. 1(b). An example of how the profile $I(\theta - \theta_B)$ transforms with the field is shown in Fig. 3.

A sharp cutoff of the intensity was not observed for all measured fields due to both the large contribution of the diffuse scattering and the spin-wave damping. The expected steplike intensity profile is somewhat smeared into the smoothly decreasing curve. Nevertheless, the increase of the field results in shrinking the spots and in shifting the cutoff angle θ_C toward θ_B. The measured intensity can be fitted by the product of the sigmoid function and the Lorentz function, which captures the main features of the scattering:

$$I(\theta) = \frac{I_0}{\theta^2 + \kappa^2}\left\{\frac{1}{2} - \left(\frac{1}{\pi}\arctan\left[\frac{2(\theta - \theta_C)}{\delta}\right]\right)\right\}. \quad (3)$$

Here the Lorentz function describes the contribution of the diffuse scattering and its parameter $\kappa^2 = \theta_0(H - H_{c2}/E_n)$ reflects the closeness of the system to the critical field H_{c2}. The sigmoid serves as a steplike function with cutoff angle θ_C, which is smeared over its width δ. It is related to the spin-wave damping as $\Gamma \approx \delta E_i$, when the instrumental resolution allows us to distinguish it.

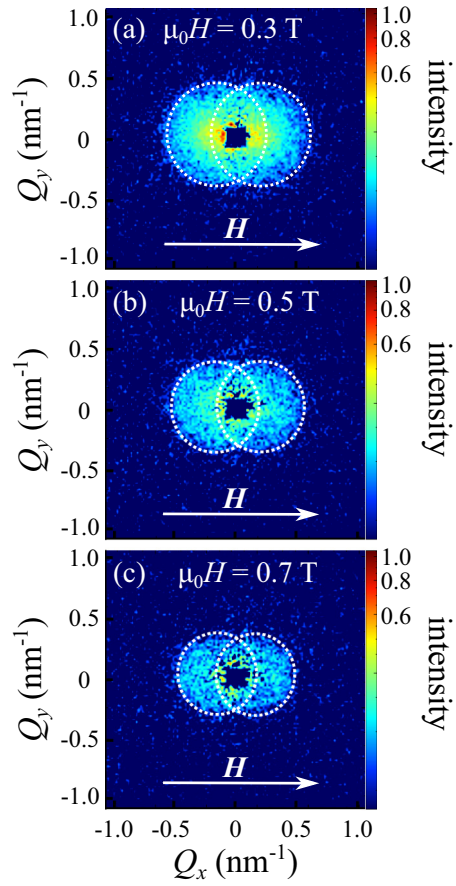

FIG. 2. Maps of the small-angle neutron scattering at the temperature $T = 15$ K for $Fe_{0.7}Co_{0.3}Si$ at different magnetic fields: (a) $\mu_0 H = 0.3$ T, (b) $\mu_0 H = 0.5$ T, (c) $\mu_0 H = 0.7$ T.

All the experimental data at different fields and temperatures were fitted by the expression Eq. (3). The extracted values of the cutoff angle (squared) θ_C^2 are plotted for $T = 15$ K as a function of the field in Fig. 4. As one can see, the square of the cutoff angle depends linearly on the field in accordance

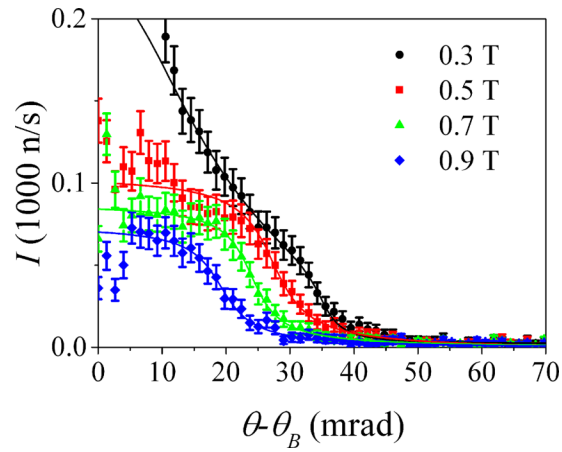

FIG. 3. Azimuth averaged neutron scattering intensity as a function of the scattering angle $(\theta - \theta_B)$ at different magnetic fields $\mu_0 H = 0.3, 0.5, 0.7, 0.9$ T for $Fe_{0.7}Co_{0.3}Si$ composition at the temperature $T = 15$ K.

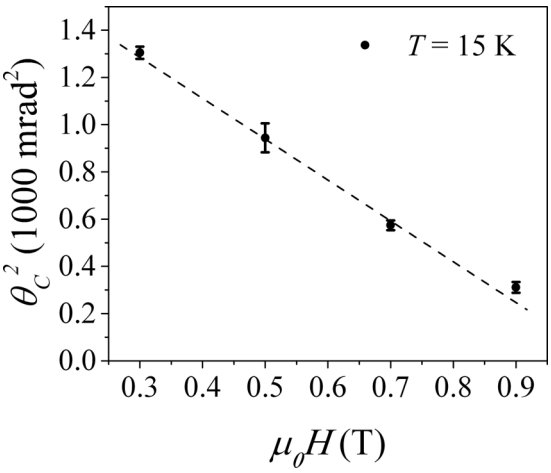

FIG. 4. The field dependence of the square of the cutoff angle θ_C^2 for $Fe_{0.7}Co_{0.3}Si$ at $T = 15$ K.

to Eq. (2). This fact ensures that the value of θ_0 (and the spin-wave stiffness A) can be determined with high accuracy as all values of θ_C taken at different fields but at the same temperature should give the same value of θ_0 upon solving Eq. (2). The approximation shows that the parameter δ related to the damping varies slightly with an increase in the field and an error of its determination increases.

The cutoff angle θ_C extracted from the fit is plotted in Fig. 5(a) as a function of temperature. Taken at a certain field value (say, $H = 0.3$ T) it increases smoothly as temperature increases. On the other hand, values of the cutoff angle θ_C are different for different magnetic fields at the same temperature in accordance to Fig. 3 and Eq. (2). One should note that the magnetic field more affects the cutoff angle at high temperatures (close to T_C) than at low and intermediate temperatures. In accordance to Eq. (2), it is related to the value of θ_0 that becomes bigger with temperature. For this reason, the magnetic field up to 1.2 T was applied for the temperatures equal to or above $T = 30$ K and it was limited by 0.9 T for measurements with T lower than 30 K. The width δ associated with the spin wave damping was normalized to θ_C plotted in Fig. 5(b). The ratio δ/θ_C is of the order of 0.2 at low temperatures and it increases with the temperature and approaches to 1 at the critical temperature range.

The fitting procedure provides the value of the parameter θ_C with an error associated with a mismatch between the measured intensity and the model function [Eq. (3)]. Using Eq. (2) one can determine the value of θ_0 and, therefore, the spin-wave stiffness A with a certain error bars for each value of the magnetic field. In spite of the fact that the cutoff angles θ_C are different for various magnetic fields (see Fig. 5) the values of the stiffness A lay close to each other (for the same temperature and different fields). Finally, all values of the spin-wave stiffness A obtained at different values of magnetic field were averaged. The error bars for the averaged value of A were calculated as a standard deviation. The temperature dependence of thus averaged spin-wave stiffness A is presented in Fig. 6.

The SANS measurements performed for the $Fe_{0.5}Co_{0.5}Si$ compound brings the scattering maps at different temperatures

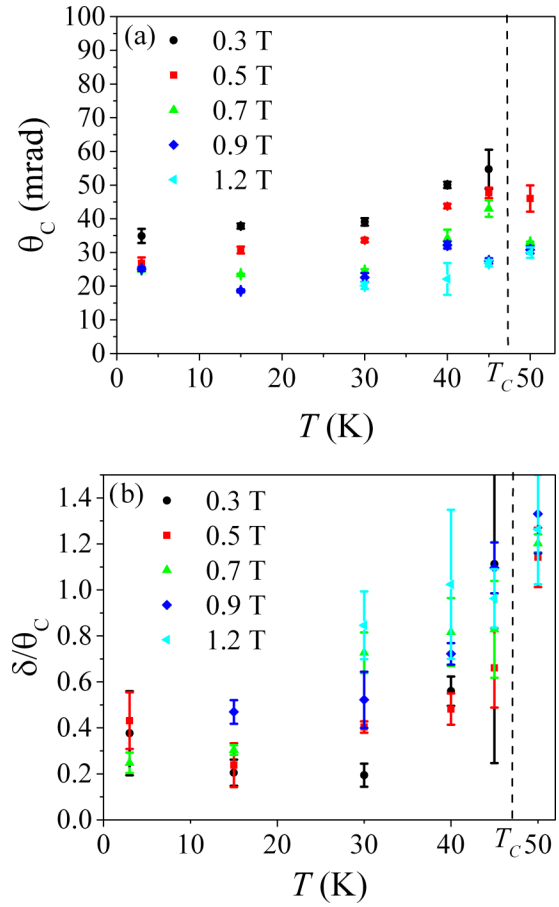

FIG. 5. (a) The temperature dependence of the cutoff angle θ_C at different magnetic fields for $Fe_{0.7}Co_{0.3}Si$ compound. (b) The ratio δ/θ_C as a function of temperature at different magnetic fields.

and fields similar to those shown in Figs. 1 and 2. The size of the inelastic scattering intensity spots is two times smaller than for the $Fe_{0.7}Co_{0.3}Si$ compound. The neutron scattering data gives the value of the spin wave stiffness A shown in

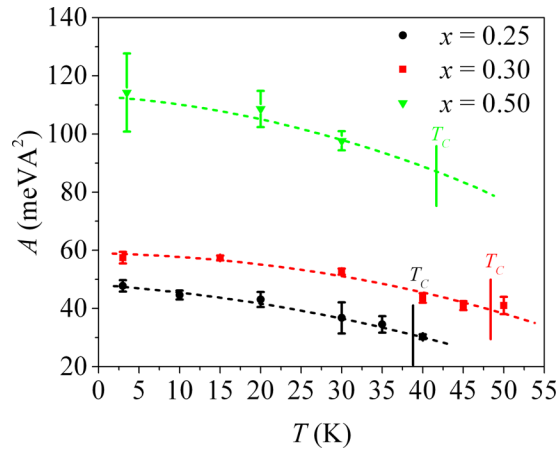

FIG. 6. The temperature dependence of the spin-wave stiffness for the three compounds $Fe_{1-x}Co_xSi$ with $x = 0.25, 0.30, 0.50$. All values of the spin-wave stiffness A obtained at different magnetic field were averaged.

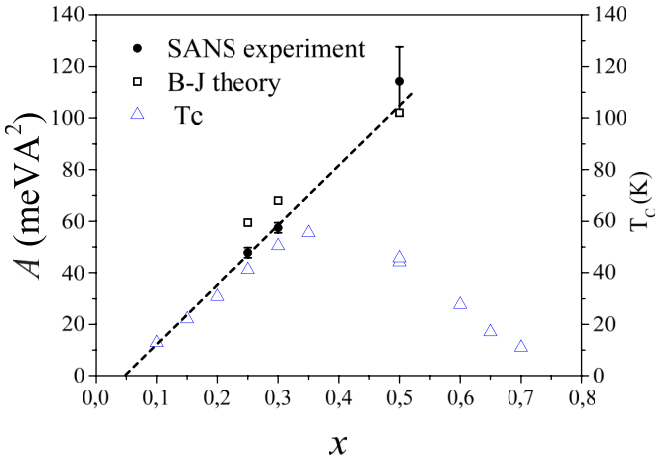

FIG. 7. The spin-wave stiffness dependence A on the concentration x for the $Fe_{1-x}Co_xSi$ compounds: data of SANS experiments extrapolated to $T = 0$ K (circles), values estimates from Bak-Jensen theory (squares). The x dependence of the critical temperature T_c (triangles) is plotted for comparison.

Fig. 6. The temperature dependence of A for the $Fe_{0.75}Co_{0.25}Si$ compound is added to Fig. 6 for completeness [29].

For all three compounds one observes a tendency for softening with temperature but the value of A at T_c remains finite. The spin wave stiffness A depends weakly on the temperature and its value near the critical temperature T_c is of the order of 0.6–0.7 of its value at 0 K.

The concentration dependence of the spin wave stiffness for the $Fe_{1-x}Co_xSi$ compounds is shown in Fig. 7. Although we have obtained three experimental points only, all of them lay very well on the linear dependence $A(x)$ that drops to zero at $x = 0.05$. This is the concentration x where the system becomes magnetically ordered. The spin waves stiffness can be estimated from the relation between the critical magnetic field H_{c2} and the energy difference $g\mu_B H_{C2} = Ak_s^2$ between the induced ferromagnetic state and helimagnetic states [20,21]. We add the estimated values to Fig. 7. As one can see they follow more or less the tendency given by the experiment: The spin wave stiffness of the $Fe_{1-x}Co_xSi$ compounds shows a linear dependence of A on the concentration x.

This x dependence of A is fully correlated with the critical temperature T_C in the range of $x \in [0.05 \div 0.4]$ [13]. The correlation between A and T_c is not surprising. It had been observed, for example, in $Mn_{1-x}Fe_xSi$ [31]. As the critical temperature T_c shows a slightly asymmetric bell-like shape function on x with a maximum at $x \sim 0.40$, these two values A and T_c are not connected above $x = 0.4$. The discrepancy between A and T_C becomes dramatically large for the Co-rich compounds (see Fig. 7).

It is instructive to compare the magnetic properties of the $Fe_{1-x}Co_xSi$ compounds with those of $Fe_{1-x}Co_xGe$ compounds [16,19]. In the Co-rich compounds the magnetic properties duplicate each other: The CoGe and CoSi are both nonmagnetic semimetals with intriguing properties [32], the ordered magnetism emerges with 80% of the Co content, the sign of the DM interaction changes at $x = 0.6$ in $Fe_{1-x}Co_xGe$ [16] and at $x = 0.65$ in $Fe_{1-x}Co_xSi$ [13], the critical temperature decreases monotonously with increase of x from 0.4 to 0.8. Thus, these two systems shows the same magnetic behavior in the Co-rich ends of the phase diagram. On the contrary, the Fe-rich compounds are different: FeGe is helimagnetic metal with very high T_c, while FeSi is nonmagnetic semiconductor. The Co doping results in the decrease of the critical temperature and the average magnetic moment for the $Fe_{1-x}Co_xGe$ compounds, while 5% of Co doping results in appearance of the helimagnetic structure in the $Fe_{1-x}Co_xSi$ compounds. Nevertheless the magnetic and transport properties of the Fe-rich part of the $Fe_{1-x}Co_xSi$ phase diagram are rather well understood [22,33–35], but the Co-rich part remains a puzzle.

There is intriguing hypothesis describing differences between magnetism in the Fe-rich and Co-rich compounds of $Fe_{1-x}Co_xSi$ [36]. It was shown that the spin dimensionality is changed by Co doping in the $Fe_{1-x}Co_xSi$ system: from the three-dimensional ($3D$) Heisenberg model for $x = 0.3$ to the $3D - XY$ model for $x = 0.5$ and to the $3D$-Ising model for $x = 0.6$. In the authors' opinion, the lowering of the spin dimensionality with the increase of Co content should result from the enhancement of the anisotropic magnetic interaction induced by the doping of Co [36]. It has been demonstrated that in the B20 compounds, the magnetism correlates closely with the structure, and the DMI in $Fe_{1-x}Co_xSi$ can be effectively controlled by the Co composition [13]. Thus, the change of spin dimensionality induced by the doping of Co should be caused by the modulation of the Dzyaloshinskii-Moriya interaction.

IV. CONCLUSION

In conclusion, we have used the recently approved SANS method [23] in order to experimentally measure the spin-wave stiffness A in the series of three compounds $Fe_{1-x}Co_xSi$ with $x = 0.25$, 0.3, and 0.5. We have found that the spin-wave stiffness A is weakly dependent on temperature. On the other hand, the spin-wave stiffness A increases linearly with x resembling the x dependences of the critical temperature T_c in the Fe-rich concentration range and strongly deviating from it in the Co-rich compounds. Obtained values of the stiffness A demonstrate quantitative applicability of the Bak-Jensen model for the $Fe_{1-x}Co_xSi$ compounds for $x = 0.25, 0.30$, and 0.50.

ACKNOWLEDGMENT

The authors are grateful for the support of the Russian Science Foundation (Grant No. 17-12-01050).

[1] O. Nakanishia, A. Yanase, A. Hasegawa, and M. Kataoka, Solid State Commun. **35**, 995 (1980).

[2] P. Bak and M. H. Jensen, J. Phys. C **13**, L881 (1980).

[3] S. Muhlbauer, B. Binz, F. Jonietz, C. Pfleiderer, A. Rosch, A. Neubauer, R. Georgii, and P. Boni, Science **323**, 915 (2009).

[4] C. Pfleiderer, T. Adams, A. Bauer, W. Biberacher, B. Binz, F. Birkelbach, P. Boni, C. Franz, R. Georgii, M. Janoschek, F. Jonietz, T. Keller, R. Ritz, S. Muhlbauer, W. Munzer, A. Neubauer, B. Pedersen, and A. Rosch, J. Phys.: Condens. Matter **22**, 164207 (2010).
[5] S. V. Grigoriev, N. M. Potapova, E. V. Moskvin, V. A. Dyadkin, Ch. Dewhurst, and S. V. Maleyev, JETP Lett. **100**, 238 (2014).
[6] J. Beille, J. Voiron, and M. Roth, Solid State Commun. **47**, 399 (1983).
[7] J. Beille, J. Voiron, F. Towfiq, M. Roth, and Z. Y. Zhang, J. Phys. F: Met. Phys. **11**, 2153 (1981).
[8] K. Ishimoto, H. Yamaguchi, Y. Yamaguchi, J. Suzuki, M. Arai, M. Furusaka, and Y. Endoh, J. Magn. Magn. Mater. **90–91**, 163 (1990).
[9] K. Ishimoto, Y. Yamaguchi, J. Suzuki, M. Arai, M. Furusaka, and Y. Endoh, Physica B **213–214**, 381 (1995).
[10] S. V. Grigoriev, S. V. Maleyev, V. A. Dyadkin, D. Menzel, J. Schoenes, and H. Eckerlebe, Phys. Rev. B **76**, 092407 (2007).
[11] S. V. Grigoriev, V. A. Dyadkin, D. Menzel, J. Schoenes, Yu. O. Chetverikov, A. I. Okorokov, H. Eckerlebe, and S. V. Maleyev, Phys. Rev. B **76**, 224424 (2007).
[12] W. Münzer, A. Neubauer, T. Adams, S. Mühlbauer, C. Franz, F. Jonietz, R. Georgii, P. Böni, B. Pedersen, M. Schmidt, A. Rosch, and C. Pfleiderer, Phys. Rev. B **81**, 041203(R) (2010).
[13] S.-A. Siegfried, E. V. Altynbaev, N. M. Chubova, V. Dyadkin, D. Chernyshov, E. V. Moskvin, D. Menzel, A. Heinemann, A. Schreyer, and S. V. Grigoriev, Phys. Rev. B **91**, 184406 (2015).
[14] S. V. Grigoriev, N. M. Potapova, S.-A. Siegfried, V. A. Dyadkin, E. V. Moskvin, V. Dmitriev, D. Menzel, C. D. Dewhurst, D. Chernyshov, R. A. Sadykov, L. N. Fomicheva, and A. V. Tsvyashchenko, Phys. Rev. Lett. **110**, 207201 (2013).
[15] K. Shibata, X. Z. Yu, T. Hara, D. Morikawa, N. Kanazawa, K. Kimoto, S. Ishiwata, Y. Matsui, and Y. Tokura, Nat. Nanotechnol. **8**, 723 (2013).
[16] S. V. Grigoriev, S.-A. Siegfried, E. V. Altynbayev, N. M. Potapova, V. Dyadkin, E. V. Moskvin, D. Menzel, A. Heinemann, S. N. Axenov, L. N. Fomicheva, and A. V. Tsvyashchenko, Phys. Rev. B **90**, 174414 (2014).
[17] T. Koretsune, N. Nagaosa, and R. Arita, Sci. Rep. **5**, 13302 (2015).
[18] J. Gayles, F. Freimuth, T. Schena, G. Lani, P. Mavropoulos, R. A. Duine, S. Blügel, J. Sinova, and Y. Mokrousov, Phys. Rev. Lett. **115**, 036602 (2015).
[19] T. Kikuchi, T. Koretsune, R. Arita, and G. Tatara, Phys. Rev. Lett. **116**, 247201 (2016).
[20] S. V. Maleyev, Phys. Rev. B **73**, 174402 (2006).
[21] A. N. Bogdanov, U. K. Roessler, and C. Pfleiderer, Physica B **359–361**, 1162 (2005).
[22] N. Manyala, Y. Sidis, J. F. DiTusa, G. Aeppli, D. P. Young, and Z. Fisk, Nature (London) **404**, 581 (2000).
[23] S. V. Grigoriev, A. S. Sukhanov, E. V. Altynbaev, S.-A. Siegfried, A. Heinemann, P. Kizhe, and S. V. Maleyev, Phys. Rev. B **92**, 220415(R) (2015).
[24] M. Kataoka, J. Phys. Soc. Jpn. **56**, 3635 (1987).
[25] Y. Iguchi, S. Uemura, K. Ueno, and Y. Onose, Phys. Rev. B **92**, 184419 (2015).
[26] S. Seki, Y. Okamura, K. Kondou, K. Shibata, M. Kubota, R. Takagi, F. Kagawa, M. Kawasaki, G. Tatara, Y. Otani, and Y. Tokura, Phys. Rev. B **93**, 235131 (2016).
[27] T. J. Sato, D. Okuyama, T. Hong, A. Kikkawa, Y. Taguchi, T. Arima, and Y. Tokura, Phys. Rev. B **94**, 144420 (2016).
[28] The data reduction software used is Graphical Reduction and Analysis SANS Program (GRASP), www.ill.eu/en/users/support-labs-infrastructure/software-scientific-tools/grasp/.
[29] S. V. Grigoriev, K. A. Pshenichnyi, E. V. Altynbaev, S.-A. Siegfried, A. Heinemann, D. Honnecker, and D. Menzel, JETP Lett. **107**, 640 (2018).
[30] N. M. Chubova, E. V. Moskvin, V. A. Dyadkin, and S. V. Grigoriev, J. Surf. Invest.: X-Ray, Synchrotron Neutron Tech. **8**, 1020 (2014).
[31] S. V. Grigoriev, E. V. Altynbaev, S.-A. Siegfried, K. A. Pschenichnyi, D. Menzel, A. Heinemann, and G. Chaboussant, Phys. Rev. B **97**, 024409 (2018).
[32] D. Takane, Z. Wang, S. Souma, K. Nakayama, T. Nakamura, H. Oinuma, Y. Nakata, H. Iwasawa, C. Cacho, T. Kim, K. Horiba, H. Kumigashira, T. Takahashi, Y. Ando, and T. Sato, Phys. Rev. Lett. **122**, 076402 (2019).
[33] M. Klein, D. Zur, D. Menzel, J. Schoenes, K. Doll, J. Röder, and F. Reinert, Phys. Rev. Lett. **101**, 046406 (2008).
[34] N. Manyala, Y. Sidis, J. F. DiTusa, G. Aeppli, D. P. Young, and Z. Fisk, Nat. Mater. **3**, 255 (2004).
[35] N. Manyala, J. F. DiTusa, G. Aeppli, and A. P. Ramirez, Nature (London) **454**, 976 (2008).
[36] L. Zhang, D. Menzel, H. Han, C. Jin, H. Du, J. Fan, M. Ge, L. Ling, C. Zhang, L. Pi, and Y. Zhang, Europhys. Lett. **115**, 67006 (2016).